Accepted Manuscript

Title: Electrochemical heavy metal detection, Photocatalytic, Photoluminescence, Biodiesel production and Antibacterial activities of Ag-ZnO nanomaterial

Author: G. Nagaraju Udayabhanu Shivaraj S.A. Prashanth M. Shastri K.V. Yathish C. Anupama D. Rangappa

PII: S0025-5408(16)30543-8
DOI: http://dx.doi.org/doi:10.1016/j.materresbull.2017.05.043
Reference: MRB 9362

To appear in: *MRB*

Received date: 10-8-2016
Revised date: 19-5-2017
Accepted date: 19-5-2017

Please cite this article as: G. Nagaraju, S.A. Prashanth, M. Shastri, K.V. Yathish, C. Anupama, D. Rangappa, Electrochemical heavy metal detection, Photocatalytic, Photoluminescence, Biodiesel production and Antibacterial activities of Ag-ZnO nanomaterial, *Materials Research Bulletin* (2017), http://dx.doi.org/10.1016/j.materresbull.2017.05.043

Electrochemical heavy metal detection, Photocatalytic, Photoluminescence, Biodiesel production and Antibacterial activities of Ag-ZnO nanomaterial

G. Nagaraju[a*],Udayabhanu[a], Shivaraj[a], S. A. Prashanth[b], M.Shastri[c], K. V. Yathish[a],C. Anupama[d], D. Rangappa[c],

[a]*Department of Chemistry, Siddaganga Institute of Technology, Tumkur, Karnataka, India.*
[b]*Department of Chemistry, Central College Campus, Bangalore University, Bengaluru, India*
[c]*Department of Nanoscience and Nanotechnology, VTU Muddenahalli, Karnataka, India.*
[d]*Department of Biotechnology, Siddaganga Institute of Technology, Tumkur, Karnataka, India.*

Abstract

Zinc oxide nanoparticles (ZnO Nps)and silver doped zinc oxide nanoparticles (Ag-ZnO Nps) were prepared using nitrates of zinc and silver as oxidizers and succinic acid as a fuel through solution combustion synthesis (SCS) at 400 ^{0}C. The synthesized materials were characterized by various analytical techniques such as XRD,FTIR, Raman UV-Vis, PL, SEM, EDX and TEM. The synthesizednanomaterials were tested for the photocatalytic degradation of methylene blue and the result reveal that Ag-ZnO Nps shows the better photocatalytic activitycompared to undoped ZnO Nps. Biodiesel production from*simarouba* oil shows that Ag-ZnO Nps acts as good catalyst compare to ZnO Nps, we have also developed sensor which showed a linearity in the concentration range50-350 nM and limit of detection was found to be 3.5 and 3.8 nM (3σ) for lead and cadmium respectively. Further we have examined the antibacterial activity against *E .coli, and S. aureus* bacteria.

Keywords: A. semiconductors; B. luminescence; C. X-ray diffraction; D. catalytic property.

Corresponding Email address: nagarajugn@rediffmail.com

1. Introduction

Nanotechnology tailoring the composition, size and shape of materials in nanometer scale to attain distinctive properties, which can be efficiently manipulated for the required applications[1]. In the current scenario, synthesizing different kinds of hybrid metal oxide nanomaterials attracts young researcher because of its novel application in almost all the fields[2, 3]. Among transition metal oxide, ZnO nanomaterialsfinds uses in a number of fields, such as ceramics, piezoelectric transducers, chemical sensors, anti-UV additives, photocatalysts, photoelectric fields etc. In addition to ZnO photocatalyst, $(BiO)_2CO_3$ and Graphitic carbon nitride based nanocomposites also acts as good photocatalysts [4-6]. ZnO Nps also shows very good antibacterial activity [7] and as a catalyst for biodiesel production[8]. Pure ZnO shows n-type conductivity, but doping changes to p-type conductivity and modifies the optical and electronic properties of the ZnO, which in turn influence the photocatalytic activity and other related applications[9-11].Lot of research groups used doped and undoped ZnO Nps as photo catalyst for the degradation of organic dye. It was found that undoped ZnO shows lower photocatalytic activity than doped ZnO Nps. This is because electron–hole pair recombination is higher in undopedbut lower in case of doped ZnO Nps[12]. In order to increase the photocatalytic activity and other applications of ZnO, noble metal incorporation to the ZnO have been carried out by various researchers [13, 14]. They synthesized noble metal doped ZnO using various method and observed improved performance compared to undoped ZnO Nps. They have suggested that both ZnO and Ag-ZnO are nontoxic in nature and finds various biological and photocatalytic applications[15]. Various methods have been used for the synthesis of ZnO Nps, few of them are co-precipitation method[16], hydrothermal method[17],sol-gel method[18], sonochemical method [19],electrodeposition[20], solid state reaction method [21], solution

combustion method[22], etc.. Among them solution combustion method is simple, rapid, energy saving and easy to scale up. It does not require any special instruments and gives pure crystalline product [23]. The obtained material is examined for the photocatalytic activity of methylene blue dye major component present in paper industry. The existence of dyes in water has become a serious issue because of its carcinogenic nature, i.e., it creates several environmental problems on the health of mankind and also to the aquatic creatures. So remediation of adverse effects of dyes in water is a very important issue today. Various techniques are available for the removal of dyes present in the wastewater. Amongst photocatalytic degradation of dyes using UV/sunlight is one of the most prominent technique because photocatalytic researchers show more inclination to carry out the reaction under ambient conditions with simple and low cost. [24]. Photocatalysis occurs on the surface of semiconductor and its efficiency is strongly influenced by morphology and surface modification of the oxide. Band gap containing semiconductor creates electron-hole pairs, electrons were generated in the conduction band and holes were generated in the valence band [25].Some of these charge carriers spread to the crystal surface and react with the adsorbed water molecules, hydroxide ions and oxygen molecules to generate reactive oxygen species, which are responsible for photo catalysis. We have also detected heavy metal ions such as lead and cadmium which are toxic in nature. The presence of these metals in the environment cause neurological, cardiovascular, reproductive disorders, kidney damage and other disorders on human health. Hence, measurement of these metal ions at trace concentration level is required. Several methods are available to detect these metal ions at trace level concentration. But, compare to other methods, electrochemical detection is more feasible[26].

In this paper we have synthesized ZnO and Ag-ZnO Nps through a simple combustion method, using nitrates of Zn and Ag as an oxidizers and succinic acid used as a fuel. Succinic

acid is nontoxic, low cost, and rich in carbon, hydrogen and oxygen. The characterized nanoparticles were used as a catalyst for the degradation ofmethylene blue (MB), electrochemical sensor for the detection of lead and cadmium, as a catalyst for biodiesel production and also used to examine the antibacterial activity.

2. Experimental

2.1. Preparationof ZnO and Ag-ZnO Nps

In order to prepare of ZnO and Ag-ZnO Nps by combustion method, zinc nitrate and silver nitrate were used as oxidizer and succinic acid as a fuel. Stochiometric ratios of 1:1 zinc nitrates and succinic acid are taken in petridish containing 15 mL H_2O. The solution is stirred to get homogeneous solution. These mixtures is introduced into preheated muffle furnace maintained at 400 ^oC,smolderingtype of combustion reaction taken place and within 5 min, nanocrystalline ZnO is formed. The product is calcined at 500^oC for 3 hour. Similar procedure was carried out for preparation of Ag-ZnO Nps by taking 5 mol % of $AgNO_3$.

2.2. Characterization

X-ray diffraction (XRD) data were recorded in Philips X'pert PRO X-ray diffractometer with graphite monochromatized Cu-Kα (1.542 Å) radiation.The Fourier transform infrared spectra (FTIR) of the samples were collected using Bruker Alpha-p spectrometer.Raman spectra were recorded 514.5 nm Ar^+ laser in HORIBA LabRam HR800 spectrometer.The absorption spectraof the samples were measured on a Perkin Elmer Lambda-750 UV–vis spectrometer.Photoluminescence (PL) spectra were examined by Agilent Cary Eclipse Fluorescence spectrometer using Xe lamp with an excitation wavelength of 397 nm.The surface morphology was observed using Carl Zeiss ultra 55 scanning electron microscope

(SEM).Transmission electron microscopy (TEM) was performed JEOL JEM 1200 Ex operating at 100 Kv and attached with EDX.

2.3. Photocatalytic degradation of dye

The photocatalytic activity studies of synthesized ZnO and Ag-ZnO Npswere evaluated bythe degradation of Methylene blue (MB) aqueous solution at room temperature using a 120 W mercury lamp as radiance source. In a typical procedure, 50, 100, 150 and 200 mg of photocatalyst was added to 100 mL of different concentration ofMB aqueous solutions (5, 10, 15 and 20 ppm) in a 150 x 75 mm sized batch reactor and the distance between the light source and the sample was maintained at 18 cm. The solution wasconstantly stirred in the dark for 30 minutes to ensure the organization of an adsorption-desorption equilibrium between the MB and photocatalyst previous to irradiation. 2 mL of thesuspension was withdrawn from the solution mixture at a sequence of 30 minutes time intervals. The dispersed ZnO/Ag-ZnO photocatalyst was removed using spinwin microcentrifuge.The rate of degradation of MB dye was monitored by measuring absorbance using UV-vis spectrophotometer at 663 nm wavelength. The percentage of degradation can be calculated using the formula.

$$\% \text{ of degradation} = \frac{C_i - C_f}{C_i} \times 100 \quad \text{..... (i)}$$

Where C_i and C_f are the initial and final concentration of the dye.

2.4. Procedure for the modification of electrode and electrochemical study:

2.4.1. Experimental

All electrochemical measurements were carried out using electrochemical work station [CH Instruments, Texas, USA, model: CHI 619B] at room temperature(25 ± 2ºC) in an

electrochemical cell of volume 10 mL with a standard three electrode configuration where modified glassy carbon electrode acts as working electrode, a platinum wire as auxiliary electrode and Ag/AgCl acted as the reference electrode. All the solutions were degassed using high purity nitrogen gas for 7-8 min. before all electrochemical measurements. pH measurements were carried out using pH meter (Control Dynamics, Mumbai, India model: APX 175).An ultrasonic bath was used for the sonication.

2.4.2. Surface modification

10 mg of Ag-ZnO was dispersed in 5 mL distilled water by ultrasonication for about 15 min to give a uniform suspension. Prior to modification, the glassy carbon electrode (GCE) was mechanically polished with alumina slurry of different grades to mirror finish then rinsed and sonicated for about 1 min in distilled water followed by ethanol. Subsequently, the dispersed suspension (5 µL) was drop coated onto the surface of the glassy carbon electrode and allowed to evaporate at room temperature. The ZnO modified GCE was prepared by the same procedure.

2.4.3. Analytical procedure

Electrochemical measurements of Pb^{2+} and Cd^{2+} was carried out using DPASV in the potential range -1.0 to 0.0 V with an amplitude of 0.01 V and pulse width of 0.05 s. Known amounts of analytes were taken in an electrochemical cell of 10 mL- volume capacity. The Ag-ZnO modified electrode was immersed into the cell containing 0.1 M KCl, buffer solution (pH 5) and target metal ions which was stirred for 2 min to preconcentrate the metal ions at open circuit potential.Then, the preconcentrated metal ions were reduced at a reduction potential of -1.2 V and subsequently stripped off from the electrode surface into the bulk of the electrolytic solution by sweeping the potential in the positive direction after 20 s of equilibration time.

2.5. Antibacterial activity

The prepared ZnO and Ag-ZnO Nps were tested for their antibacterial activity by following Kirby-Bauer disk diffusion method[27, 28]against one Gram-negative bacteria Escherichia coli (MTCC45) and one Gram-positive bacteria Staphylococcus aureus (MTCC3160). The inoculum was prepared by transferring a loop full of culture from the stock to tubes containing Mueller-Hinton broth (MHB) at 37°C on a rotary shaker at 200 rpm until absorbance reached around 0.4 to 0.6 at 600 nm to ensure that cells are in exponential phase. Muller Hilton agar media was prepared and poured into sterile Petri plates and allowed it to solidify. The above sub cultured broth of respective organisms was swabbed on the solidified MH agar plates and allowed to dry for about 10 min. The wells were punched on the plates using cork borer of diameter 6mm. 200mg of sample was dissolved with 1 ml of deionized water and it is placed in an ultrasonicator for 30 min to break intermolecular interactions. Now ZnO and Ag-ZnO Nps were finally containing disaggregated particles and used as standard concentration. From same, different volumes like 50µl and 100µl, of samples added to each wells. Standard antibiotic streptomycin is taken with volume of 50µl (5mg/ml of final concentration) as positive control and 50 µl of water as negative control. Then the plates were incubated at 37°C for 18-24 hrs. For development of inhibition zones. After incubation time the zones of inhibition were observed and diameters of the zones were measured and tabulated. All plates are done in triplicates.

2.6. Biodiesel synthesis

The transesterification reaction was carried out in a 1 liter three neck flask equipped with a reflex condenser, thermostat, mechanical stirrer, sampling outlet and mechanical stirrer set at 650 rpm. 500 mL of simarouba oil was added to the flask and preheated the oil before the

reaction started. 1.5% w/v ZnO is added to the methanol (9:1 methanol to oil molar ratio) and the resultant mixture was added to the preheated oil and reaction mixture was maintained at 64 ^{o}C by digital thermometer and reaction was carried out for a period of 2 hours. After completion of the reaction, the reaction mixture was transferred to separating funnel and allowed to settle for overnight. The catalyst, glycerin and biodiesel were separated, unreacted methanol was recovered from biodiesel and obtained biodiesel was filtered to remove any dissolved zinc oxide catalyst. Similar procedure was carried for Ag-ZnO Nps.

3. Results and discussion

The XRD pattern of ZnO and Ag-ZnO Nps prepared by solution combustion method is depicted in Fig. 1.The XRD pattern of pure ZnO(Fig. 1a) shows diffraction peaks, that can be indexed to the hexagonal wurtzite structure with lattice parameters a=b=3.2498 Å and c=5.2066 Å, Theobtained data arein good agreement with the JCPDS no. 36-1451.The XRD pattern of Ag-ZnONps(Fig. 1b)shows the additional peaks compared to bare ZnO Nps at 2θ values 38.2, 44.2 and 64.3 corresponds tocubic phase silver (JCPDS no. 2-109) [29].The average crystallite size calculated using Debye-Scherrer equation was found to be 19 and 37 nm for ZnO and Ag-ZnO Nps respectively.

$$D = \frac{0.89\lambda}{\beta \cos\theta} \text{.....(}ii\text{)}$$

D is the crystallite size,λ is the wavelength of the X-ray source,β is the full width at half maximum,θ is the Braggs diffracting angle.

The FTIR spectrum of ZnO and Ag-ZnO Nps was recorded in the range 350-4000 cm^{-1}, and it is given in Fig. 2. From the FTIR spectrum, various functional groups and metal-oxide bond present in the compound were analyzed. In the FTIR spectrum, a significant vibration band ranging from 400cm^{-1}to 500 cm^{-1} is assigned to the characteristic stretching mode of Zn-O bond.

In the case of Ag-ZnO Nps the intensity of peak is reduced due to the formation of Ag nanoparticles on the surface of ZnO Nps [30] . A broad peak at 3434 cm^{-1} (stretching) and 1330$cm^{-1}$to 1670 cm^{-1} (bending) indicates the presence of hydroxyl residue which is due to atmospheric moisture [31,32].

To investigate the influence of Ag on the molecular vibrational modes of ZnO Nps, room temperature Raman spectra of ZnO and Ag-ZnO Nps were recorded in the spectral range of 200 to 1000 cm^{-1}, as shown in figure S1**.** The Raman spectrum of undoped ZnO Nps (figure S1a) consist of peaks that were observed at 331 cm^{-1} (second-order vibration), 438, 517 and 580 cm^{-1}, corresponding to the E_{2H}-E_{2L}, E_{2H}, E_1(TO)+ E_{2L}, E_1 (LO), fundamental phonon modes of hexagonal ZnO, respectively. The 331 cm^{-1} mode could be observed by enhancement of Raman active and inactive phonons, with lattice symmetry due to disorder-activated Raman scattering. The E_2 mode at 438 cm^{-1} mode corresponds to wurtzite structured ZnO, and a very sharp feature. The vibration at 537 cm^{-1} can be attributed to either a local vibration mode related to the donor defects or oxygen vacancies and Zn interstitials. The 580 cm^{-1} E_1 (LO) corresponds to well resolve Raman peaks due to multiphonon and resonance processes, and are related to oxygen deficiency. Ag-ZnO composite related vibrational modes were identified at 346 and 508 cm^{-1}. Decrease in intensity of Raman spectrum of Ag-ZnO Nps (figure S1b) is due to the incorporation of Ag into ZnO Nps. The incorporation of defects/impurity may breakdown of translational crystal symmetry [33, 34]

UV-Vis spectra were recorded from 200 to 800nm range and is as shown in Fig. S2.Ag-ZnO Nps (Fig.S2 (b).) shows an intense peak at 388 nm indicated to band gap of 3.19 eV and pure ZnO(Fig.S2 (a).) shows an intense peak at 377 nm corresponds to a band gap of 3.29 eV.The red shift in the UV-Vis spectrum of Ag-ZnO Nps compare to

pure ZnO nanoparticles clearly shows the reduction in the band gap [35]. Due to the lesser band gap of Ag-ZnO Nps, it shows higher photocatalytic activity for degradation of dye compared to the undoped ZnO Nps.

Photoluminescence study is one of the beneficial technique to find the efficiency of charge carrier separation in the semiconductor[36].Fig. 3 shows the PL emission spectrum of ZnO and Ag-ZnO Nps were recorded at the room temperature with an excitation wavelength of 397 nm. The pure ZnO Nps gives a strong UV emission peak at 542 nm and weak emission peak at 485 nm. In case of Ag-ZnO Nps, the obtained PL emission intensity decreased and these results are in good agreement with the Stern-Volmer quenching. This indicates higher charge carrier separation efficiency in the case of Ag-ZnO Nps. The obtained emission peaks are in the visible region could be ascribed to bound excitons and defect states positioned at surface of nanostructured pure and doped ZnO Nps respectively. The inset of (Fig. 3.) gives PL excitation spectrum with emission at 542 nm [37]. The chromaticity co-ordinates is used to find out the luminous color of material. It can be estimated using Commission International De I'Eclairage (CIE) system. Fig. S3. shows the CIE chromaticity diagram of ZnO and Ag-ZnO Nps and clearly shows that both the materials emits blue light region

Fig. S4 shows the SEM images of ZnO and Ag-ZnO Nps. It clearly shows that they are agglomerated and almost spherical in shape. In case of Ag-ZnO Nps (Fiig. S4, e,d) the presence of bright Ag particles on the surface of ZnO. TEM images (Fig. 4) showed almost spherical shape. The average size of the ZnO and Ag-ZnO Nps were found to be 24 nm and 42 nm respectively. The HRTEM image of Ag-ZnO NPs as shown in Fig. 4f reveals that interplanar spacing of 0.27 nm corresponds to growing directions of ZnO along (101) and 0.21 nm

corresponds to the Ag along (200) direction. EDS analysis. (Fig. S5) clearly shows the presence of Ag atoms in addition to Zn and O in Ag-ZnO Nps.

Fig. 5 (a_1&a_2)shows the effect of catalytic load of ZnO and Ag-ZnO Nps on the photocatalytic degradation efficiency of methylene blue dye of 10ppm atpH-7. The result shows that, as the catalyst dosage increases, efficiency of degradation also increases in both the cases. This is due to the fact that, as the catalytic weight increases, number of active sites on surface of catalyst also increases which in turn increases the number of holes and hydroxyl radicals, resulting in rapid degradation. Further increasing of catalytic load, sedimentation and agglomeration of the particles takes place and turbidity of slurry increases and thereby decreases the light penetration, which automatically decreasing the number of holes and hydroxyl radicals.

The effect of pH on the photocatalytic degradation of methylene blue dye was shown inFig. 5 (b1& b2). Degradation process mainly depends on the pHof the solution [38].Variation of pH changes the surface properties of both ZnO and Ag-ZnO Nps, which alters the degradation efficiency. The highestphotocatalytic degradation efficiency was observed in basic medium compare to acidic medium.At higher pH more number of hydroxyl radicals are formed which increases the degradation efficiency in both the cases at pH-9. The obtained result was good agreement with the reported studies [39, 40].

Fig. 5 (c_1&c_2)shows the effect of dye concentration (5-20 ppm)on the photocatalytic degradation of methylene blue by keeping catalytic load of 100 mg and atpH 7. The obtained results shows that, as the concentration of dye solution increases, degradation efficiency decreases. This is due to more number of dye molecules were adsorbed on the surface of catalyst, leads to decrease in active sites of catalyst.It clearly shows that maximumdegradation efficiency is at 5 ppm dye solution.

Fig.S6 (a&b)shows the comparison study of photocatalytic activity of ZnO and Ag-ZnO Nps under both UV and sunlight exposure. By taking constantmethylene blue dye concentration of 10 ppm,catalytic load of 100mg and pH 7, the highest degradation efficiency was observed in Ag-ZnO Nps followed by ZnO Nps. This is due to efficient charge separation occurs in the case of Ag-ZnO Nps. Fig. S6 (c)shows the kinetic study on photocatalytic degradation of methylene blue dye using both pure and Ag-ZnO Nps. These are follows pseudo first order rate law for degradation of dye and rate constant was calculated using the equation.

$$K = (2.303X \text{ slope}) \ldots\ldots\ldots\ldots \text{(xiii)}$$

Rate constant was found to be $2.9x10^{-2}$ and $2.08x10^{-2}$ min^{-1} for ZnO and Ag-ZnO Nps respectively.

It clearly shows that the rate of a reaction is more in the case of Ag-ZnO Nps compared to undoped ZnO Nps.

The mechanisms underlying the enhanced photocatalytic activity of Ag–ZnO hybrid plasmonic nanostructures towards the degradation of MB can be understood as follows: The SPR of Ag nanoparticles helps in extending the light absorption of ZnO from near UV to the visible region, leading to an improved light utilization efficiency. In addition, decoration with Ag nanoparticles significantly improves the charge separation in ZnO. When ZnO absorbs photons of energy greater than or equal to its band gap, electrons are promoted from its valence band to conduction band, creating equal number of holes in the valence band. Since the energy level of conduction band of ZnO is higher than the Fermi level of Ag–ZnO hybrid structure, electrons flow from ZnO nanostructures to Ag nanoparticles. Hence Ag nanoparticles act as efficient sinks for the photogenerated electrons, preventing their recombination with holes. This process, known as the direct electron transfer from semiconductor to the plasmonic nanostructures, is dependent on the

alignment of electronic band structure of the noble metal and semiconductor. Furthermore, irradiation with light leads to the excitation of MB dye molecules adsorbed onto the ZnO nanostructures. The photoexcited MB molecules transfer electrons into the conduction band of ZnO. The photogenerated electrons created by the above mentioned processes react with dissolved O_2 molecules forming superoxide anion radicals, while holes react with H_2O leading to the formation of hydroxyl radicals, both of which cause the degradation of the MB dye [41, 42]. Mechanisms of formation of possible radicals are as shown in Eqs. (iii) – (xii) and scheme.1.

$$O_2 + e^- \rightarrow O_2^- \quad \text{(iii)}$$

$$O_2^- + H^+ \rightarrow HO_2^{\bullet} \quad \text{(iv)}$$

$$HO_2^{\bullet} + HO_2^{\bullet} \rightarrow H_2O_2 + O_2 \quad \text{(v)}$$

$$H_2O_2 + e^-_{CB} \rightarrow HO^{\bullet} + HO^- \quad \text{(vi)}$$

$$H_2O_2 + O_2^- \rightarrow HO^{\bullet} + HO^- + O_2 \quad \text{(vii)}$$

$$H_2O_2 \rightarrow 2HO^{\bullet} \quad \text{(viii)}$$

$$O_2 + HO^- \rightarrow O_2^- + HO^{\bullet} \quad \text{(ix)}$$

$$\text{Dye} + HO^{\bullet} \rightarrow \text{Degradation products} \quad \text{(x)}$$

$$\text{Dye} + h^+_{VB} \rightarrow \text{oxidation products} \quad \text{(xi)}$$

$$\text{Dye} + e^-_{CB} \rightarrow \text{reduction products} \quad \text{(xii)}$$

Detection of$OH^{\bullet}$formed during the photocatalytic degradation reaction using spectrofluorometer for Ag-ZnO Nps is shown in theFig. S6 (d). We used coumarin as probe molecule in the present study because when coumarin react with $OH^{\bullet}$changes the chemical structure to produce highly-fluorescent 7-hydroxyl coumarin. The experimental procedure for fluorescent probe method is by dispersing 200 mg Ag-ZnO in 50 mL of 1 mM coumarin solution. The above solution was stirred vigorously for 30 min before light irradiation.Every 10 min, aliquots were taken out and the PL intensity was measured with excitation wavelength of320 nm. It clearly shows that intensity increases linearly with irradiation time, which indicated the formation of $OH^{\bullet}$ during photocatalytic degradation at the surface of Ag-ZnO Nps [43].

Electrochemical behavior of ZnO and Ag-ZnO Nps: Simultaneous measurement of Pb^{2+} and Cd^{2+} ions.

Electro catalytic behavior of ZnO and Ag-ZnO Nps modified glassy carbon electrode has been examined using electrochemical techniques such as cyclic voltammetry (CV) and differential pulse anodic stripping voltammetry (DPASV). Fig.6 (a) depicts the CVs of Pb^{2+} and Cd^{2+}ions at modified and unmodified (bare) electrodes Furthermore no peak current signals were obtained for bare glassy carbon electrode (BGCE) in absence of metal ions, whereas at modified glassy carbon electrodes a significant anodic and cathodic signals were obtained in presence of 10mM of Pb^{2+} and Cd^{2+}ions in a acetate buffer solution of pH 5 with a scan rate of 50mV/s. However the modified glassy carbon electrode has not shown any current signals for the oxidation of zinc into zinc ions. Hence this could be used as an electrochemical interface for the measurement of Pb^{2+} and Cd^{2+}ions. However CVs were recorded in the potential window from -1.40 to 0.10 V and in presence of 10 mM of metal ions at ZnO (Fig. 6 a,b)and Ag doped ZnO (Fig. 6 a, c) modified electrodes to distinguish the electro catalytic activity of the electrodes. The

CVs were recorded at bare BGCE (Fig. 6 a, a) in presence of 10 mM of metal ions and it has showed a tiny peak current at a peak potential of -0.78V which might be due the reduction of extraneous ions which were present in 10 mL capacity of the electrochemical cell, whereas the ZnO modified GCE in same composition has showed a significant peak current at a peak potential of 0.45 and -0.78V which is due the oxidation of Pb^{2+} and Cd^{2+} ions and the reduction peak potentials were observed at -0.44 and -0.81V respectively. Furthermore the Ag-ZnO modified GCE has been examined in the same domain and the anodic peak current signals were significantly enhanced for Pb^{2+} and for Cd^{2+} a small peak current has obtained. From this it can be concluded that the use of Ag-ZnO nanoparticle modified electrode can be used for the quantification of Pb^{2+} and Cd^{2+} ions.

In order to achieve the maximum efficiency of the Ag-ZnO modified electrode in the electrochemical quantification of metal ions DPASV were used. Fig. 6 (b).Shows the *simultaneous* detection Pb^{2+} and Cd^{2+} ions in presence of 50 – 300 nM in a pH 5 of acetate buffer solution at an applied potential of -1.20 V. In order to enhance the analytical signal the metal ions were measured separately and it has shown in Fig. 6 (c) and (d).

To examine the analytical applicability of the developed interface for the quantification of metal ions from various industrial and environmental samples [44]. It is adequate to construct a calibration plot with the standard solutions of target analytes. Hence the calibration plot has been constructed and showed linearity in the range 50 – 350 nM using DPASV and it has been performed by the successive addition of 50 nM of analytes into a stirred solution of acetate buffer of pH 5 at an applied potential of -1.2 V of 10 mL capacity of electrochemical cell. The response of oxidation peak current of metal ions to the variation of concentration of metal ions

increases linearly with the increase of its concentration upto 350 nM and limit of detection was found to be 3.5 and 3.8 nM (3σ) respectively.

Antimicrobial activity

The qualitative antibacterial assay was carried out by employing standardkirby-bauer disc diffusion methodagainst *E .coli, and S. aureus* and the diameter of inhibition zones were tabulated in table 1.The maximum inhibition activity was found in*Staphylococcus aureus.* The next activity was found in E.coli. Literature studies showed that the ZnO Nps and Ag-ZnO Nps are effectively act against both gram negative bacteria and gram positive bacteria [45-47], but Compare to ZnO, Ag-ZnO shows good inhibition. It shows synergic antibacterial activity found to be more prominent against Gram-positive bacteria than Gram-negative bacteria. The possible Inhibitory action is physical damage caused by interaction of the material with outer cell wall layer increased by increased concentration of Ag-ZnO Nps. It is found that more zone of inhibition was seen at a concentration of 500µg of Ag-ZnO Nps.Fig. 7shows antibacterial activity of ZnO and Ag-ZnO against *E .coli, and S. aureus* bacteria.

Biodiesel Synthesis

Biodiesel is well known as fatty acid methyl ester, an alternative fuel to diesel that has many benefits; nontoxic, renewable, environmental friendly and biodegradable [48].Currently, the homogeneous catalysts KOH/NaOH have been extensively used for the biodiesel production. But, these have several disadvantages, purification of biodiesel is difficult and requires large amount of water [49] and increase the operating and capital cost[50]. To overcome these problems, heterogeneous solid catalysts are favorable for biodiesel production and these catalysts are environmentally friendly. The main advantage of using heterogeneous catalyst is easy separation and purification of final products [51]. In the present study, simarouba oil was used

for synthesis of biodiesel using ZnO and Ag-ZnO Nps as catalysts. After transesterification process, the yield of biodiesels obtained using ZnO and Ag-ZnO Nps as catalysts was found to be 80.1 and 84.5% respectively. The Ag-ZnO Nps shows higher catalytic activity which could be a potential catalyst for biodiesel production compared to ZnO Nps. In order to assess the quality of biodiesel, fuel properties kinematic viscosity, density, flash point, copper strip corrosion and acid value were evaluated and compare with ASTM standards as shown in the table 2.

Fig. S7 shows the mechanism of heterogeneous acid catalyzed transesterification reaction [52]. The formation of more electrophilic species occurs in the first step of the reaction mechanism. In this case, rate-determining step depends on the acid catalyst strength. After formation of Lewis complex (stage1), in the 2^{nd} stage alcohol nucleophilic bonding takes place, and new ester formed in the stage 3, the new ester desorbs from the Lewis site (stage 4) and the cycle is repeated.

Among the transition metal oxides, the ZrO_2, ZnO, TiO_2 have more concerned for biodiesel synthesis due to their acidic properties [53]. Among the transition metal oxides, zinc oxide was reported as one of the best catalysts for trans-esterification due to its high activity and minimum weight loss in the reaction [54]. ZnO Nps have high catalytic activity and large surface area and this solid catalyst have more advantage to apply to a catalytic reaction in transesterification [55, 56]. The biodiesel yield is more in Ag-ZnO Nps catalyzed trans-esterification reaction compare to ZnO Nps catalyzed reaction. In trans-esterification reaction, ZnO Nps was slightly loses the weight compare to Ag-ZnO NPs, this reduces the yield of biodiesel.

Conclusion

Wehavesuccessfullysynthesized ZnO and Ag-ZnO Nps by solutioncombustionmethod using succinic acid as a low cost novel fuel.XRDpattern clearlyshowsthe presenceofAgintheZnO

matrix. FTIR spectral studies revealed avibration band ranging from 400cm^{-1}to 500 cm^{-1} is assigned to the characteristic stretching mode of Zn-O bond. In the case of Ag-ZnO Nps the intensity of peak is reduced due to formation of Ag Nps on the surface of ZnO Nps. UV–Vis absorptionspectrumof Ag-ZnO show red shift compare to ZnO Nps. PL spectrum of ZnO and Ag-ZnO Nps showed a strong UV emission at 542 nm. SEM images show thatthey areagglomerated and almost spherical in shape. EDSanalysis reveals the presence of Ag atoms in the Ag-ZnO Nps. TEM image shows that the average particle size of ZnO and Ag-ZnO Nps found to be24 and 42 nm respectively. Ag-ZnO Nps shows superior catalytic activities for the degradation of MB and biodiesel production compare to ZnO Nps. Ag-ZnO Nps also shows goodantibacterial activity. We have also succeeded for the detection of heavy metal ion Pb and Cd at nano level concentration.

Acknowledgement

Authors thank DST Nanomission, Govt. of India, New Delhi for financial support to carry out the research work (Project No. SR/NM/NS-1262/2013 (G) dated 18-03-2015). G. Nagaraju thanks BRNS-BARC, DAE, Bombay, Govt. of India for financial help to carry out the research work (37(2)/14/25/2015/BRNSdated 03/12/2015). Also acknowledges VGST, Govt. of Karnataka, for the financial help under the scheme of Seed Money to Young Scientists for research (SMYSR, GRDNumber - 498) to procure UV-Visible photoreactor. Thanks to Siddaganga Institute of Technology, Tumakuru for encouraging the research activity.

References

[1]Mariana Sima, Eugeniu Vasile, Marian Sima,ZnO films and nanorod/shell arrays electrodeposited on PET-ITO electrodes, Materials Research Bulletin. 48 (2013) 1581–1586.

[2] Xiaolan Deng, Lilan Zhang, Jing Guo, Qinjun Chen, Jianmin, ZnO enhanced NiO-based gas sensors towards ethanol, Materials Research Bulletin. 90 (2017) 170–174.

[3] Sooho Lee, Yongseob Park, Donguk Kim, Dohyun Baek, Junsin Yi, Byungyou Hong, Wonseok Choic, Jaehyeong Lee, Thermal stability of hydrogen-doped AZO thin films for photovoltaic applications, Materials Research Bulletin. 58 (2014)126–131.

[4] L. S. Mende, J. L. M. Driscoll,ZnO nanostructures, defects, and devices, Materials Today.10 (2007) 40-48.

[5] Z. Nia, Y. Suna, Y. Zhangb, F. Dong, Fabrication, modification and application of $(BiO)_2CO_3$-based photocatalysts: A review, Applied Surface Science365 (2016), 314–335.

[6] Z. Zhao, Y. Suna, F. Dong, Graphitic carbon nitride based nanocomposites: a review, Nanoscale, 7 (2015), 15-37.

[7] L. Zhang, Y. Dinga, M.Povey, D. York, ZnO nanofluids – A potential antibacterial agent, Progress in Natural Science. 18 (2008) 939-944.

[8] R. Madhuvilakku, S. Piraman, R. Madhuvilakku, S. Piraman, Bioresource technology. 150 (2013) 55-59.

[9] R. Georgekutty, M. K. Seery, S. C. Pillai, A Highly Efficient Ag-ZnO Photocatalyst: Synthesis, properties and mechanism, The Journal of Physical Chemistry C. 112(2008) 13563-13570.

[10] Kwang-Hyuk Choi, Sanghun Jeon, Han-Ki Kim, A comparison of Ga:ZnO and Ga:ZnO/Ag/Ga:ZnO source/drain electrodes for In–Ga–Zn–O thin film transistors, Materials Research Bulletin. 58 (2014) 126–131.

[11] Y. Zheng, C. Chen, Y. Zhan, X.Lin, Q. Zheng, K. Wei, J.Zhu,Photocatalytic activity of Ag/ZnO heterostructure nanocatalyst: Correlation between structure and property, The Journal of Physical Chemistry C. 112 (2008) 10773-10777.

[12]X. Yin, W. Que, D. Fei, F. Shen, Q. Guo, Ag nanoparticle/ZnO nanorods nanocomposites derived by a seed-mediated method and their photocatalytic properties, Journal of Alloys and Compounds. 524 (2012) 13-21.

[13] B.Aleksandra, Y. H. Leung, C. H.Wallace, K. W. Cheah, W. K. Chan, Visible photoluminescence in ZnO tetrapod and multipod structures, Applied Physics Letters. 84 (2004) 2635-2637.

[14] Y. Nosaka, N. Ohta, H. Miyama, Photochemical kinetics of ultrasmall semiconductor particles in solution: effect of size on the quantum yield of electron transfer, Journal of Physical Chemistry.94 (1990) 3752-3755.

[15] B.R Reed, D. A. Ladner,C. P. Higgins, P. Westerhoff, J. F. Ranville, Solubility of nano-zinc oxide in environmentally and biologically important matrices, Environmental Toxicology and Chemistry. 31 (2012) 93-99.

[16] T. Jan, J. Iqbal, M.Ismail, M. Zakaullah, S. Haider, N.N.Badshah, Sn doping induced enhancement in the activity of ZnO nanostructures against antibiotic resistant S. aureus bacteria, International journal of nanomedicine. 8 (2013) 3679-3687.

[17] G. Nagaraju, T.N. Ravishankar, K. Manjunath, S. Sarkar, H. Nagabhushana, R. Goncalves, J. Dupont, Ionothermal synthesis of TiO_2 nanoparticles: Photocatalytic hydrogen generation, Materials Letters. 109(2013) 27-30.

[18] K. Namratha, K . Byrappa, Bai, Jamuna, V.Ravishankar, Ehrentrant, Dirk,I. A. Ibrahim, M.Yoshimura, Antimicrobial Activity of Silver Doped ZnO Designer Nanoparticles, Journal of Biomaterials and Tissue Engineering. 3 (2013) 190-195.

[19] Dimple P. Dutta, A.K. Tyagi, Facile sonochemical synthesis of Ag modified Bi4Ti3O12 nanoparticles with enhanced photocatalytic activity under visible light, Materials Research Bulletin. 74 (2016) 397–407.

[20] P. S. S. Kumar, A. Manivel, S. Anandan, Synthesis of Ag-ZnO nanoparticles for enhanced photocatalytic degradation of acid red 88 in aqueous environment, Water Sci. Technol. 59 (2009) 1423-1430.

[21] Feng Zhang a, Yu Wang, Hanjun Chen, Wenlin Feng, Effects of Ag particles on sintering and electrical properties of ZnO-based varistor, Materials Research Bulletin 45 (2010) 974–978.

[22] X. Li, Y. Wang, Structure and photoluminescence properties of Ag-coated ZnO nano-needles, Journal of Alloys and Compounds. 509 (2011) 5765-5768.

[23] Udayabhanu, G. Nagaraju, H. Nagabhushana, R. B. Basavaraj, G. K. Raghu, D. Suresh, H. Rajanaika and S. C. Sharma, Green, non-chemical route for the synthesis of ZnO superstructures, Evaluation of its applications towards Photocatalysis, Photoluminescence and Bio-sensing, Crystal Growth and Design, 16 (2016) 6828-6841

[24] T.N. Ravishankar, K. Sureshkumar, J. Dupont, T. Ramakrishnappa, G. Nagaraju,Ionic liquid assisted hydrothermal synthesis of TiO_2 nanoparticles and its applications towards

the photocatalytic activity and electrochemical sensor, J. Experimental Nanoscience,10 (2015) 1358-1373

[25] X G. Hu, J. Li, C. Yu, Design, Fabrication, and Modification of Nanostructured SemiconductorMaterials for Environmental and Energy Applications, Langmuir. 26 (2010) 3031-3039.

[26] P. S. Adarakatti, P. Malingappa, Amino-calixarene-modified graphitic carbon as a novel electrochemical interface for simultaneous measurement of lead and cadmium ions at picomolar level, Journal of Solid State Electrochemistry. (2016) 1-10.

[27] A. W. Bauer, W.M. Kirby, J.C. Sherris, M. Turck, Antibiotic susceptibility testing by a standardized single disk method, American journal of clinical pathology. 45 (1966) 493.

[28]S. J. P. Jacob, J. Finub, A. Narayanan, Synthesis of silver nanoparticles using Piper longum leaf extracts and its cytotoxic activity against Hep-2 cell line, Colloids and Surfaces B: Biointerfaces. 91 (2012) 212-214.

[29] T. Wang,Z. Jiao, T. Chen, Y. Li, W. Ren, S. Lin, G. Lu, Jinhua Yec, Yingpu Bi, Vertically aligned ZnO nanowire arrays tip-grafted with silver nanoparticles for photoelectrochemical applications, Nanoscale. 5 (2013) 7552-7557.

[30] R. Zamiri, A. Rebelo, G. Zamiri, A. Adnani, A. Kuashal, M.S.Belsleyd, J. M. F. Ferreira, Far-infrared optical constants of ZnO and ZnO/Ag nanostructures, RSC Advances. 4 (2014) 20902-20908.

[31] P. Hower, T. Gupta, A barrier model for ZnO varistors, Journal of Applied Physics. 50 (1979) 4847-4855.

[32] R. Wahab, S.G. Ansari, Y.S. Kim, H. K. Seo, G. S. Kim, G. Khang, H.S. Shin, Low temperature solution synthesis and characterization of ZnO nano-flowers, Materials Research Bulletin. 42 (2007) 1640-1648.

[33] R. S. Zeferino, M. B. Flores, U. Pal, Photoluminescence and Raman Scattering in Ag-doped ZnO Nanoparticles, J. of Applied Physics 109 (2011) 014308-16.[

[34] A. H. Shah, E. Manikandan, M. B. Ahmed, V. Ganesan, Enhanced Bioactivity of AgZnO Nanorods-A Comparative Antibacterial Study, J. NanomedNanotechol. 4 (2013) 1000168

[35] O. A. Yıldırım, H. E. Unalan, C. Durucan, . Highly Efficient Room Temperature Synthesis of Silver-Doped Zinc Oxide (ZnO:Ag) Nanoparticles: Structural, Optical, and Photocatalytic Properties, Journal of the American Ceramic Society. 96 (2013) 766-773.

[36] G. K. Tripathi, I. D. Sharma, C. Kant, R.R. Pandey, K. K. Saini, R. Kurchania, Characterization of the Photocatalytic Activity of Bismuth Oxychloride Nanostructures, Analytical Letters. 49 (2016) 1452-1466.

[37] S. S. Patil, M. G. Malic, M. S. Tambolia, D. R. Patil, M. V. Kulkarni, Hyun Yoon, Hayong Kim, S. S. Al-Deyabd, S. S. Yoonc, S. S. Kolekarb, B. B. Kale, Green approach for hierarchical nanostructured Ag-ZnO and their photocatalytic performance under sunlight, Catalysis Today. 260(2016) 126-134.

[38] M. Barakat, J. Tseng, C. Huang, Hydrogen peroxide-assisted photocatalytic oxidation of phenolic compounds, Applied Catalysis B: Environmental. (59)2005 99-104.

[39]L. S. Daniel, Hiroki Nagai, Naoya Yoshid, Mitsunobu Sato,Photocatalytic Activity of Vis-Responsive Ag-Nanoparticles/TiO_2 Composite; Thin Films Fabricated by Molecular Precursor Method (MPM), Catalysts, 3 (2013) 625-645.

[40] B. Patil, D. Nayak, V. Shrivastava, Use of Some Semiconductors as Photocatalyst for the Removal of o-nitro Phenol: A Kinetic Study, Journal of Applied Chemical Research. 13 (2010) 7-22.

[41] S. Kuriakose, V. Choudhary, B. Satpati, S. Mohapatra, Enhanced photocatalytic activity of Ag–ZnO hybrid plasmonic nanostructures prepared by a facile wet chemical method, J. Nanotechnol. 5 (2014) 639–650.

[42] P. Arsan, C. Bubpa, W.S. Aroon, Photocatalytic activity under solar irradiation of silver and copper doped zinc oxide: photodeposition versus liquid impregnation methods, Journal of Applied Sciences. 12 (2012)1809-1816.

[43] Q. Xiang, J. Yu, P.K. Wong, Q. Xiang, J. Yu, P.K. Wong, Quantitative characterization of hydroxyl radicals produced by various photocatalysts, Journal of Colloid and Interface Science. 357 (2011) 163-167.

[44] G. Hanrahan, D.G. Patil, Electrochemical sensors for environmental monitoring: design, development and applications, J. Wang, Journal of Environmental Monitoring. 6 (2004) 657-664.

[45] S. Medda, Deepa G. Patila, Joseph Wang, Electrochemical sensors for environmental monitoring: design, development and applications, Applied Nanoscience. (2014) 1-6.

[46] D.V. Ponnuvelu, S.P. Suriyaraj, T. Vijayaraghavan, R. Selvakumar, B. Pullithadathail, Enhanced cell-wall damage mediated, antibacterial activity of core–shell ZnO@Ag heterojunction nanorods against Staphylococcus aureus and Pseudomonas aeruginosa, Journal of Materials Science: Materials in Medicine. 26 (2015) 1-12.

[47]A. Shafaghat, Synthesis and Reactivity in Inorganic, Metal-Organic, and Nano-Metal Chemistry. 45 (2015) 381-387.

[48] F. Ma, M.A. Hanna, Biodiesel production: a review, Bioresource technology. 70 (1999) 1-15.

[49] B. Yoosuka, P.Krasaea, B. Puttasawata, P. Udomsapa, N.V. Empikulb, K. Faungnawaki,Magnesia modified with strontium as a solid base catalyst for transesterification of palm olein, Chemical Engineering Journal. 162(2010) 58-66.

[50] M. Canakci, The potential of restaurant waste lipids as biodiesel feedstocks, Bioresource Technology. 98 (2007) 183-190.

[51] G. Kafuku, M.K. Lam, J. Kansedo, K.T. Lee, M. Mbaraw, Heterogeneous catalyzed biodiesel production from Moringa oleifera oil, Fuel Processing Technology. 91 (2010) 1525-1529

[52] M. Zabeti, Wan Daud, W. M. A, K. M. Aroua, Activity of solid catalysts for biodiesel production: A review, Fuel Process Technol. 90 (2009) 770-777.

[53] SJ.Yoo, HS. Lee, V, Bambang, JD. Kim, Yw.Lee, Synthesis of biodiesel from rapeseed oil using supercritical methanol with metal oxide catalysts,Bioresour Technol. 101 (2010) 8686-9.

[54] N. K. Park, Y. J. Lee, G. B. Han,S. O.Ryu, T. J. Lee, C. H. Chang, G. Y. Han, Synthesis of various zinc oxide nanostructures with zinc acetate and activated carbon by a matrix-assisted method, Colloids and Surfaces A:Physicochemical and Engineering Aspects. 313 (2008) 66-71.

[55] A. C. Alba-Rubio,J. Santamaría-González, J. M. Mérida-Robles, R. Moreno-Tost, D. Martin-Alonso, A. Jiménez-López, P. Maireles-Torres, Heterogeneous transesterification processes by using CaO supported on zinc oxide as basic catalysts, Catal. Today. 149 (2010) 281-287.

[56] D. S. Martino, T. Riccardo, P. Lu, S. Eloi, Heterogeneous catalysts for biodiesel production, Energy and Fuels. 22 (2007) 207-217.

Figure Caption

Scheme 1: Schematic representation for degradation of Methylene blue by Ag-ZnO Nps under UV radiation.

Table. 1 The antibacterial properties of (a) ZnO (b) Ag-ZnO Nps

Table . 2. Fuel Properties of Simaroubabiodiesel using ZnO and Ag-ZnO Nps.

Fig. 1XRD pattern of (a) ZnO and (b) Ag-ZnO Nps

Fig. 2 FTIR spectrum (a) ZnO (b) Ag-ZnO Nps

Fig. 3 Photoluminescence spectrum of (a) ZnO (b) Ag-ZnO Nps [inset: Potoluminescence excitation spectrum].

Fig. 4.TEM imagesof (a-b) ZnO, (c-d) Ag-ZnO and HRTEM of (e) ZnO, (f) Ag-ZnO Nps.

Fig. 5 Effect of (a1,a2) catalytic load, (b1,b2) pH and (c1,c2) dye concentration on the photocatalytic activity of ZnO and Ag-ZnO Nps.

Fig. 6. (a) Overlaid cyclic voltammograms of bare glassy carbon electrode in absence of $Pb^{2+}$and Cd^{2+} ions (a), ZnO modified glassy carbon electrode (b) and Ag doped ZnO modified glassy carbon electrode (c) in presence of 10 mM of $Pb^{2+}$and Cd^{2+} ions in a acetate buffer solution of pH 5.0 containing 0.1 M KCl as supporting electrolyte with a scan rate of 50 mV/s. (**b)**Overlaid differential pulse anodic stripping voltammograms of the Ag doped ZnO modified electrode in presence of different concentration of Pb^{2+} and Cd^{2+} ions at -1.20 V. **(c)**Overlaid differential pulse anodic stripping voltammogram of Pb^{2+} in the concentration range 50 – 350 nM (inset calibration plot). **(d)**Overlaid differential pulse anodic stripping voltammogram of Cd^{2+} in the concentration range 50 – 350 nM (inset calibration plot).

Fig. 7. Antibacterial activity of (a,c) *E .coli* and *(b,) S. aureus using* ZnO and Ag-ZnO Nps.

Supplementary information:

Fig.S1 Raman spectrum of (a) ZnO and (b) Ag-ZnO Nps.

Fig. S2. UV-Vis spectrum of (a) ZnO and(b) Ag-ZnO Nps.

Fig. S3. CIE diagram of ZnO and Ag-ZnO Nps.

Fig. S4. SEM images of (a-b) ZnO and (c-d) Ag-ZnO Nps.

Fig. S5. EDS spectrum of (a) ZnO and (b) Ag-ZnO Nps.

Fig. S6. Comparison study of photocatalytic activity of ZnO and Ag-ZnO Nps under (a) UV and (b) sunlight exposure.**(c)** Kinetic studies on photocatalytic degradation of Methylene blue by using ZnO and Ag- ZnO Nps and **(d)** Detection of OHradicals by PL spectrum of Coumarin solution.

Fig. S7 Mechanism of heterogeneous solid acid catalyzed trans esterification (M denotes ZnO or Ag-ZnO)

Research Highlights

- For the first time reporting the ZnO and Ag-ZnO Nps through solution combustion synthesis using succinic acid as low cost novel fuel.
- Ag-ZnO Nps shows superior photocatalytic activity, antibacterial activity and biodiesel production compare to ZnO Nps.
- ZnO and Ag-ZnO Nps has been used as a electrochemical interface to detect lead and cadmium metal ions simultaneously at nano concentration level.

Graphical abstract

Electrochemical heavy metal detection, Photocatalytic, Photoluminescence, Biodiesel production and Antibacterial activities of Ag-ZnO nanomaterial

G. Nagaraju [a*], G. C. Shivaraju [a], S. A. Prashanth [b], Mahesh Shastri [c], K. V. Yathish [a], C. Anupama [d], Dinesh Rangappa [c],

[a] Department of Chemistry, Siddaganga Institute of Technology, Tumkur, Karnataka, India.

[b]Department of Chemistry, Central College Campus, Bangalore University, Bengaluru, India

[c] Department of Nanoscience and Nanotechnology, VTU Muddenahalli, Karnataka, India.

[d] Department of Biotechnology, Siddaganga Institute of Technology, Tumkur, Karnataka, India.

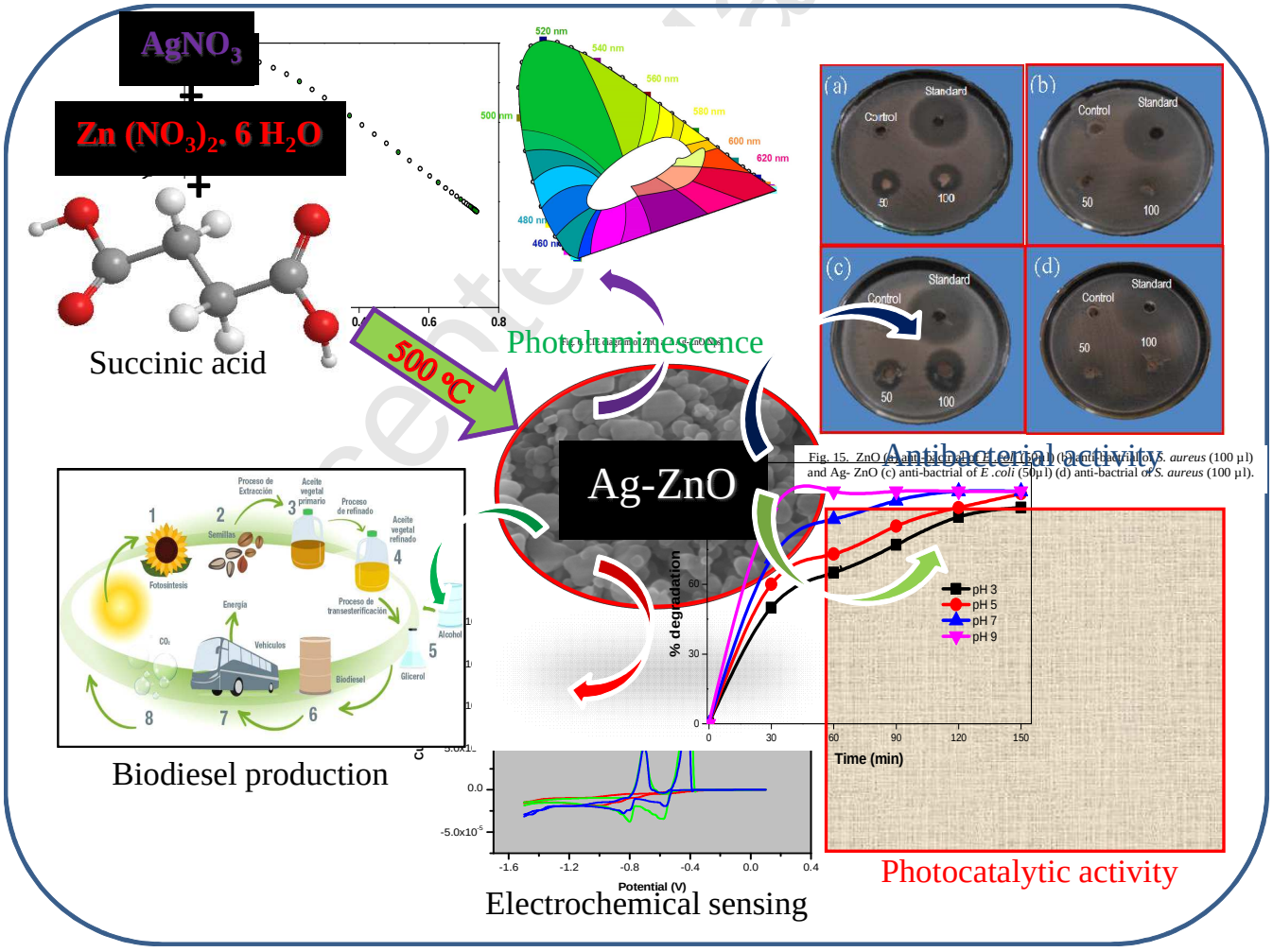

Fig. 15. ZnO (a) anti-bacterial of *E. coli* (50 µl) (b) anti-bacterial of *S. aureus* (100 µl) and Ag- ZnO (c) anti-bacterial of *E .coli* (50µl) (d) anti-bacterial of *S. aureus* (100 µl).

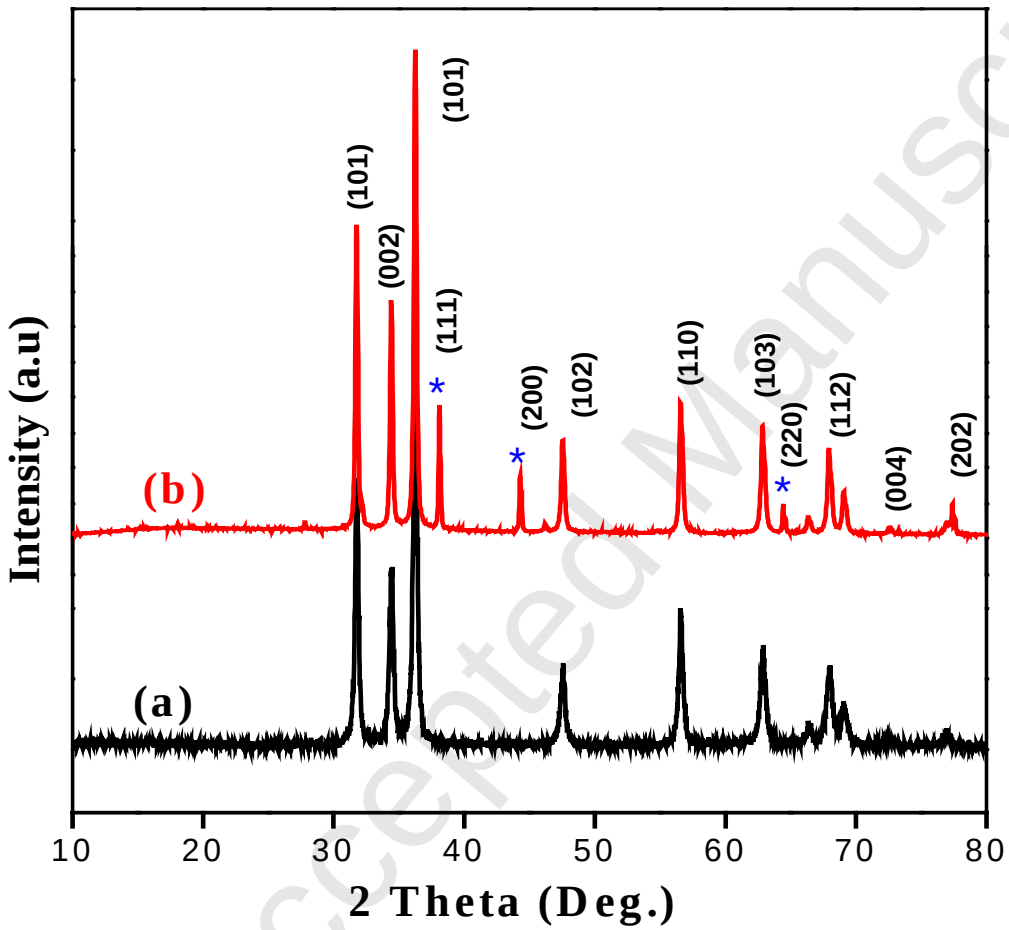

Fig. 1. XRD pattern of (a) ZnO and (b) Ag-ZnO Nps. (* indicates Ag)

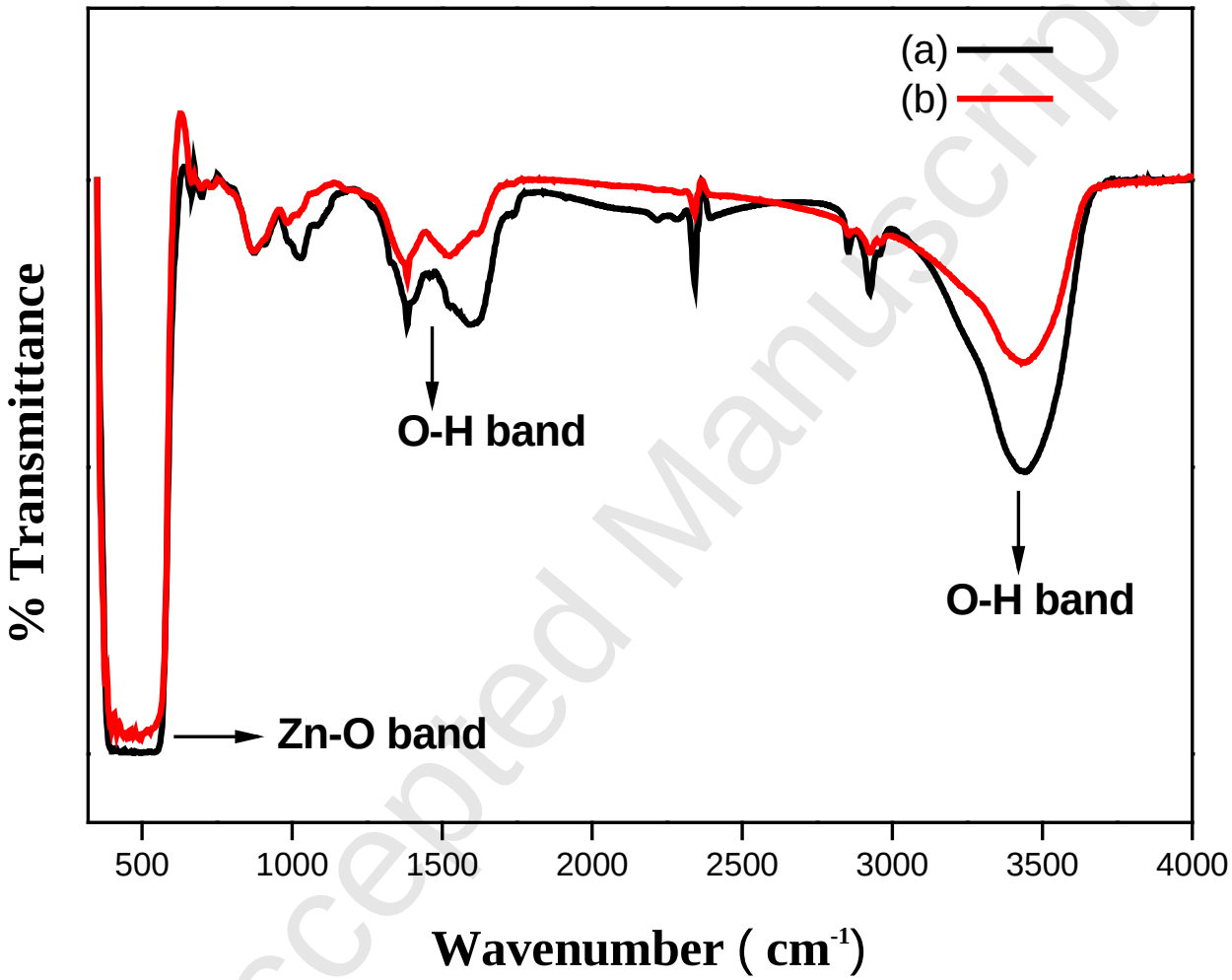

Fig. 2. FTIR spectrum of the (a) ZnO and (b) Ag-ZnO Nps.

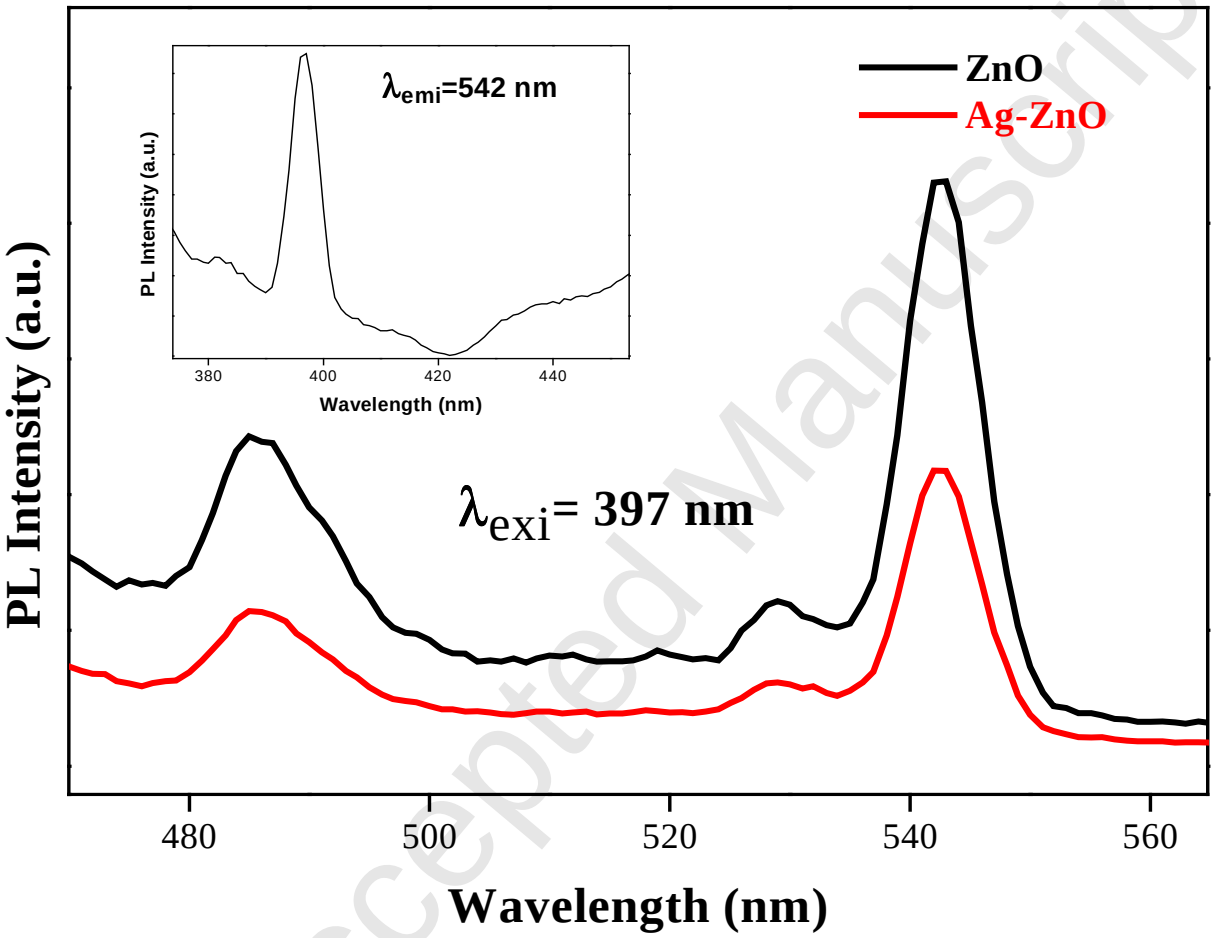

Fig. 3. Photoluminescence excitation spectrum of the (a) ZnO (b) Ag-ZnO Nps [inset gives Photoluminescence emission spectrum].

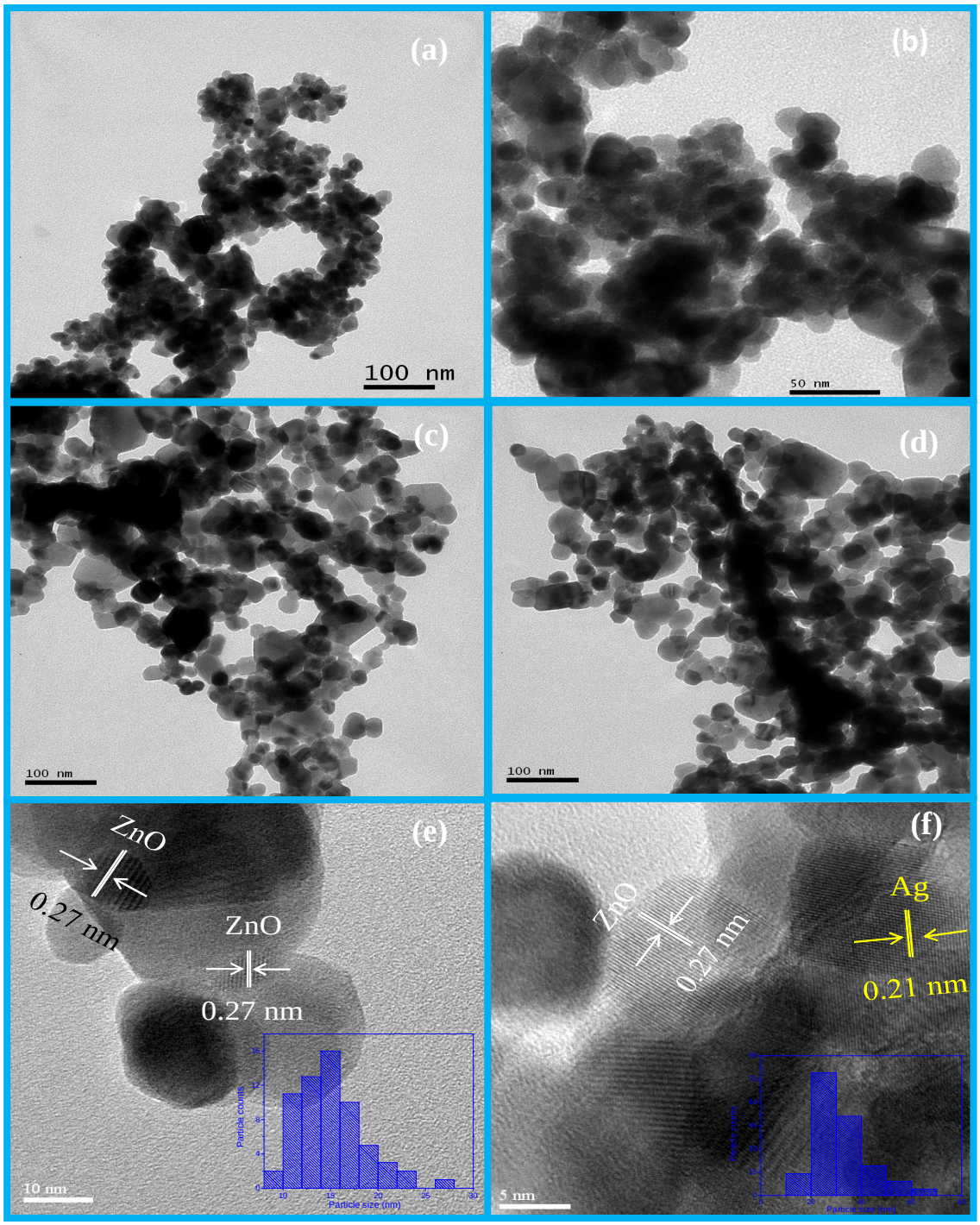

Fig. 4. TEM images of the (a-b) ZnO, (c-d) Ag-ZnO and HRTEM of (e) ZnO, (f) Ag-ZnO Nps. [Inset of (e) and (f) Histogram of ZnO and Ag-ZnO Nps]

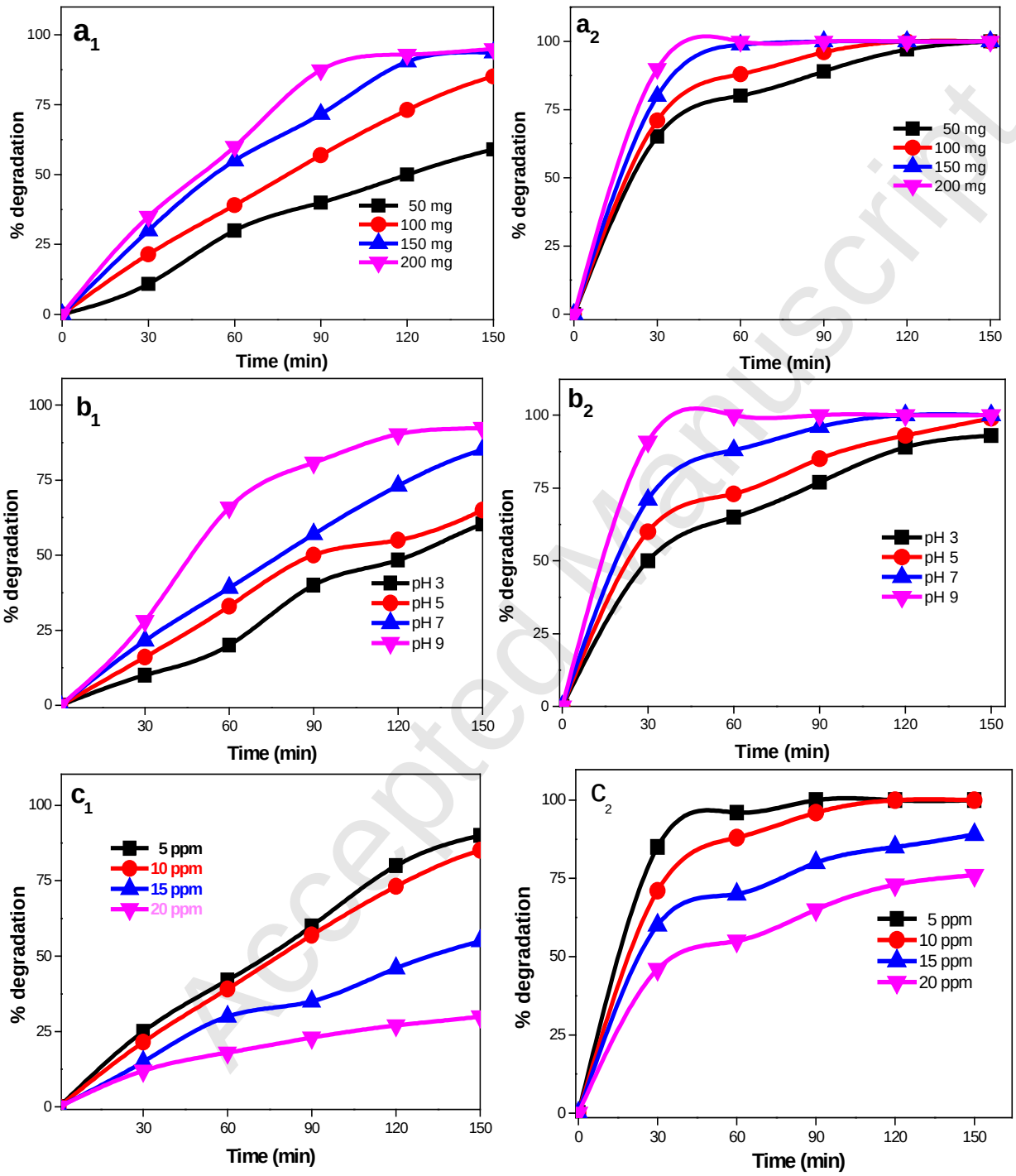

Fig. 5 Effect of catalytic dose on the photocatalytic process of (a_1) ZnO and (a_2) Ag-ZnO Nps. Effect of pH on photocatalytic process of the (b_1) ZnO and (b_2) Ag-ZnO Nps and . Effect of dye concentration on the photocatalytic process of the (c_1) ZnO and (c_2) Ag-ZnO Nps.

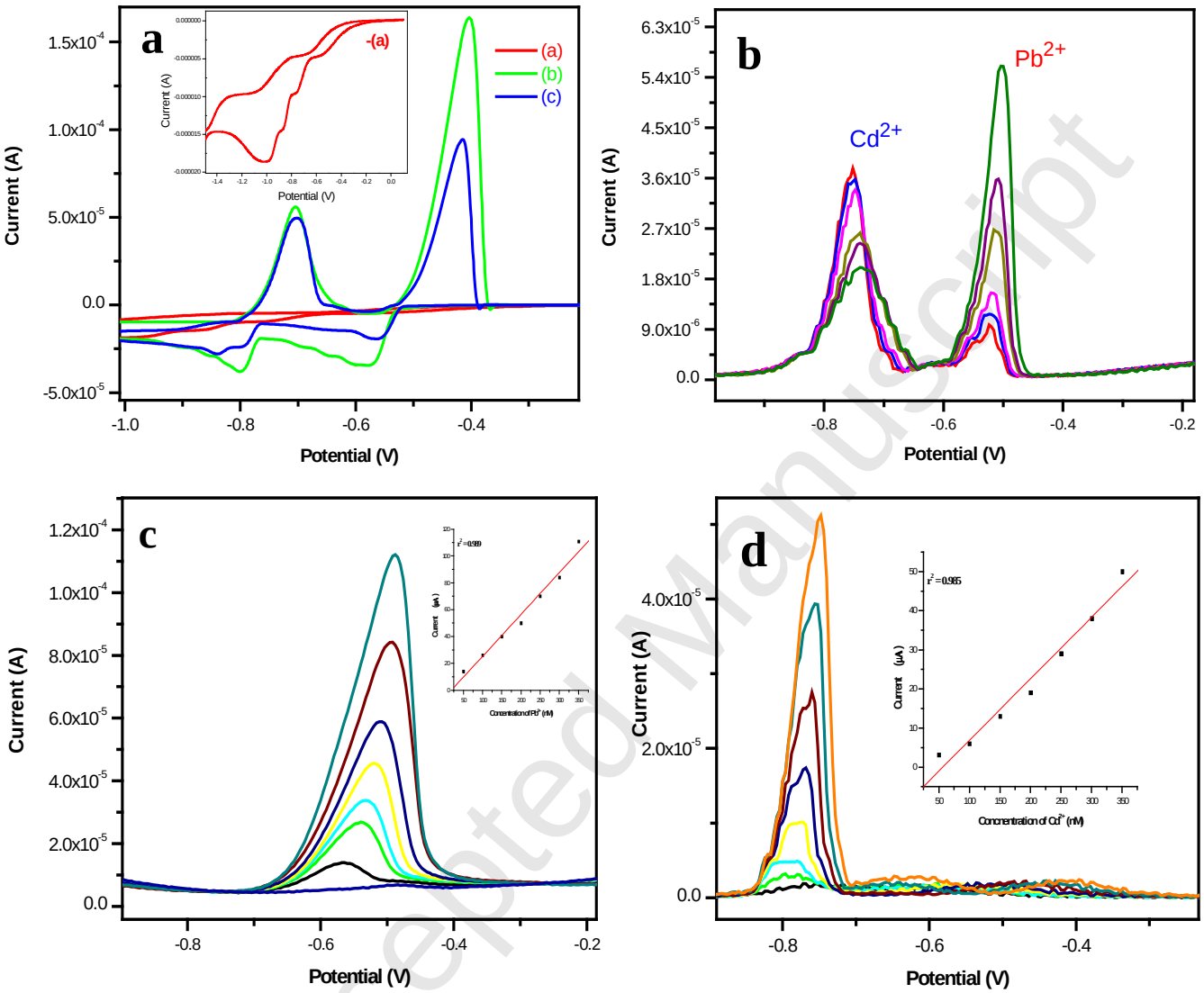

Fig. 6. (a) Overlaid cyclic voltammograms of bare glassy carbon electrode in absence of Pb^{2+} and Cd^{2+} ions (a), ZnO modified glassy carbon electrode (b) and Ag doped ZnO modified glassy carbon electrode (c) in presence of 10 mM of Pb^{2+} and Cd^{2+} ions in a acetate buffer solution of pH 5.0 containing 0.1 M KCl as supporting electrolyte with a scan rate of 50 mV/s. **(b)** Overlaid differential pulse anodic stripping voltammograms of the Ag doped ZnO modified electrode in presence of different concentration of Pb^{2+} and Cd^{2+} ions at -1.20 V. **(c)** Overlaid differential pulse anodic stripping voltammogram of Pb^{2+} in the concentration range 50 – 350 nM (inset calibration plot). **(d)** Overlaid differential pulse anodic stripping voltammogram of Cd^{2+} in the concentration range 50 – 350 nM (inset calibration plot).

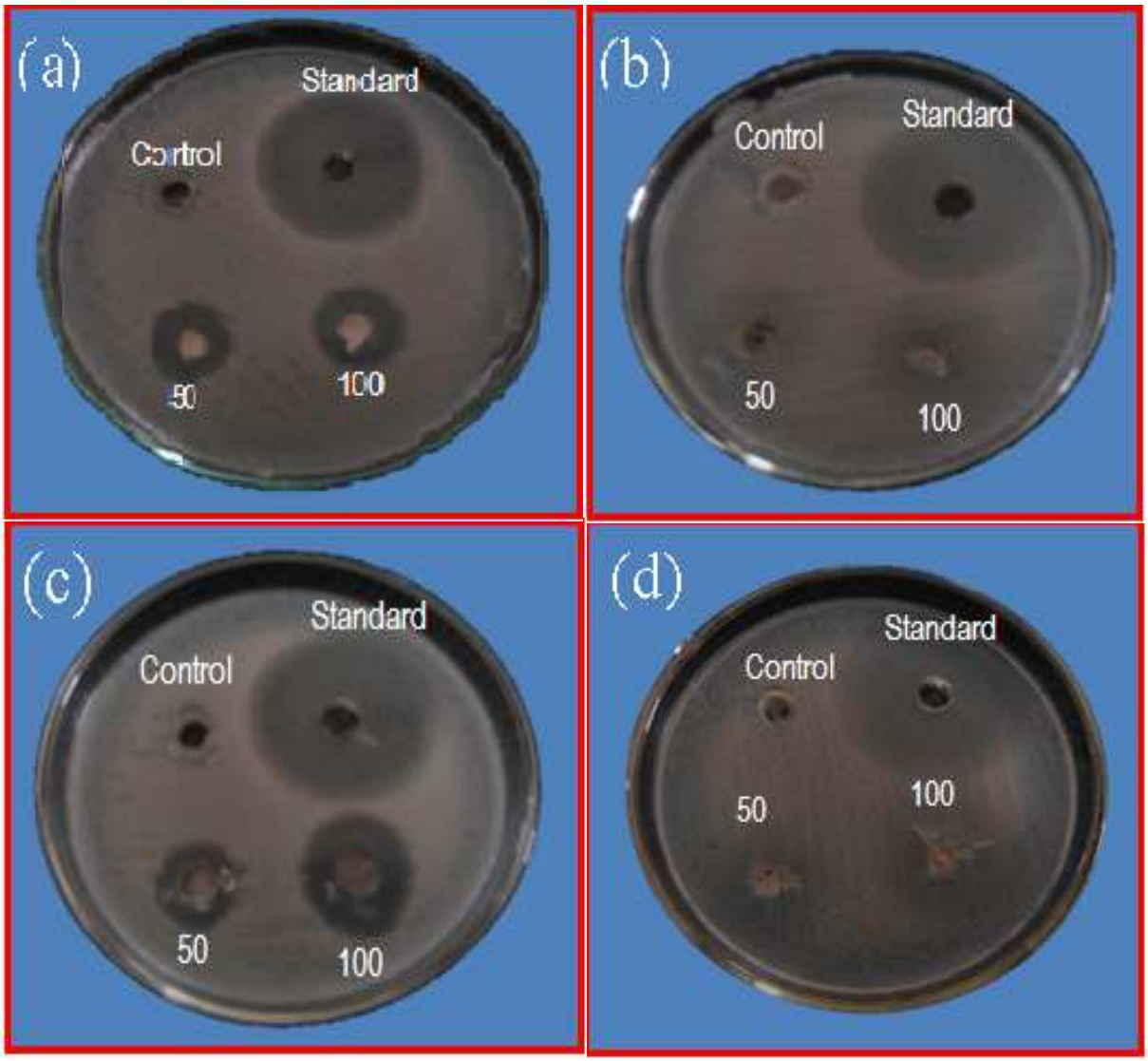

Fig. 7. Antibacterial activity of of *E .coli* (a) and *S. aureus* (b) *of* ZnO. Antibacterial activity of of *E .coli* (a) and *S. aureus* (b) of Ag-ZnO

Group	Treatment	Inhibition Zones in diameter (mm)			
		E. coli		*S. aureus*	
		50µl	100 µl	50 µl	100 µl
I	Streptomycin	39.6±0.28	39.6±0.28	30±0.57	30±0.57
II	Deionized water	No inhibition	No inhibition	No inhibition	No inhibition
III	ZnO	12.4±0.5	10.8±0.8	15±1.2	13.8±0.8
IV	Ag-ZnO	8.8±0.8	12.6±0.8	14.6±0.5	19.2±0.8

Note: Values represent the mean ± S.E. for N=3 replicates. Probability value less than 0.10 is considered as significant.

Table. 1. Antibacterial activity of ZnO and Ag-ZnO

Properties	**Units**	**Testing procedure ASTM**	**Simarouba biodiesel**		**Biodiesel standard ASTM 6751**
			ZnO catalyzed	**Ag/ZnO catalyzed**	
Viscosity at 40 ^{o}C	mm^2/sec	D445	5.1	4.9	1.9-6.0
Density	Kg/m^3	D93	890	880	870-900
Flash point	$^{\circ}$C	D4052	168	174	>130
Copper strip corrosion, 50 ^{o}C, 3h	-----	D130	1a	1a	no. 3 max
Acid value	Mg KOH/g	D664	0.7	0.62	0.8 max

Table . 2. Fuel Properties of Simarouba biodiesel using ZnO and Ag-ZnO Nps.

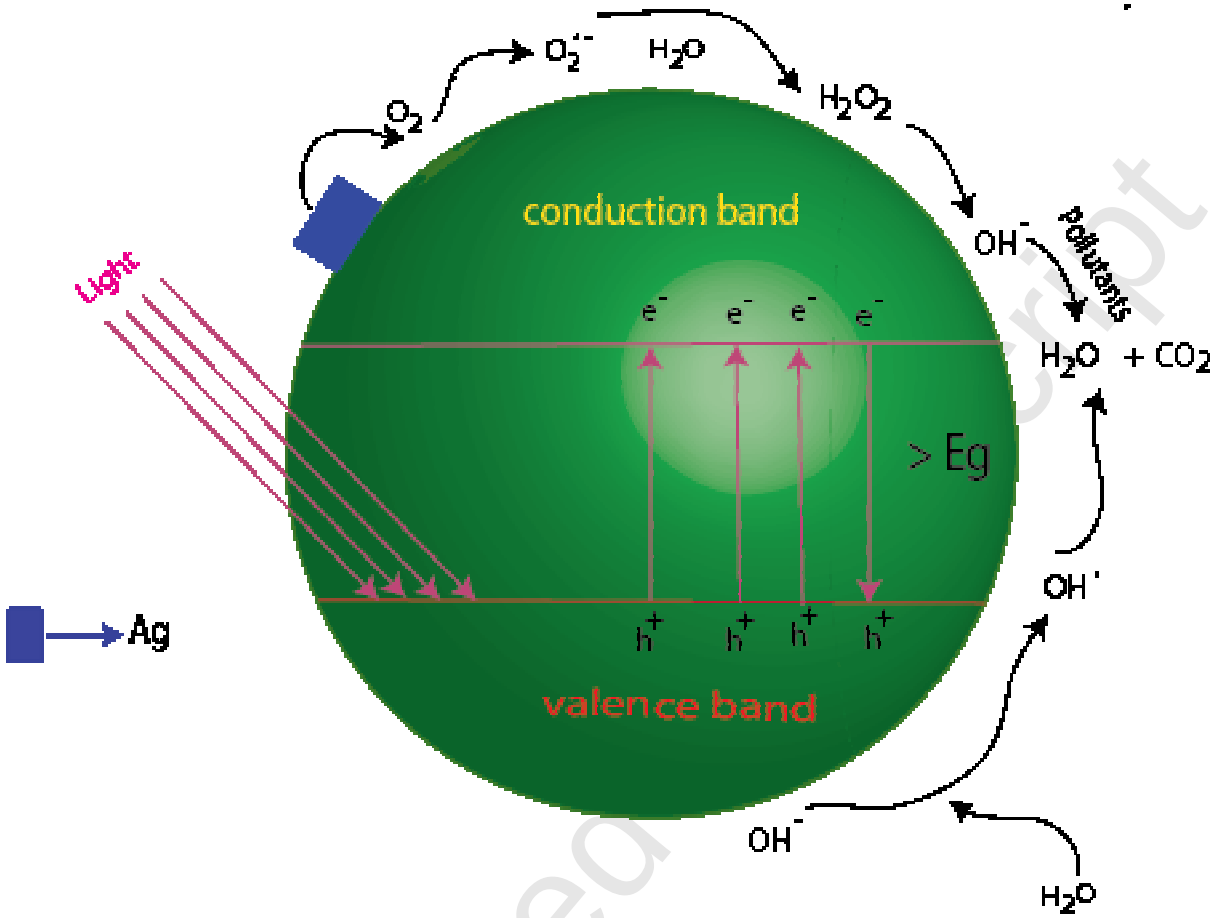

Scheme. 1. Schematic diagram of possible mechanism for photocatalytic activity of Ag-ZnO Nps for degradation of dye.